The compliance of the molecular hydride superconductor BiH$_4$ with the Migdal's theorem

E. F. Talantsev, Yu. V. Blinova, and A. V. Korolev

M. N. Miheev Institute of Metal Physics, Ural Branch, Russian Academy of Sciences, 18, S. Kovalevskoy St., Ekaterinburg 620108, Russia

Abstract

The discovery of near-room-temperature superconductivity in H$_3$S sparked experimental and theoretical studies of highly compressed hydrides with the aim of obtaining room-temperature superconductivity. There are two dominant hydride classes where the search is ongoing: the first class is the covalently bonded hydrides (which is represented by H$_3$S and H$_3$P), and the second class is the clathrate-type hydrides (which is represented by LaH$_{10}$, YH$_6$, CaH$_6$, and other). In these classes, the hydrogen ions form three-dimensional sub-lattices involving the dissociation of hydrogen molecules (where, the H-H distance is 74 pm) into a metallic state with the shortest H-H distance of 151 pm in H$_3$S and 115 pm in LaH$_{10}$. Recently, the third class of highly compressed superconducting hydrides, where the hydrogen remains its molecular form, has been discovered. This class is represented by two superhydrides, BaH$_{12}$ and BiH$_4$, which both exhibit the smallest H-H distance of 81 pm in the pressure ranges where the highest T_c is achieved. Here, we analyzed the available experimental data for the molecular hydrides BaH$_{12}$ and BiH$_4$. We found that BaH$_{12}$ exhibits nanosized grains of an average size of 26 nm and a low level of microstrain of 0.1%, both of which are independent of pressure in the range of $126\ GPa < P < 160\ GPa$. We also derived the Debye Θ_D and Einstein Θ_E temperatures, and the electron-phonon coupling constant λ_{e-ph}, in BaH$_{12}$ and BiH$_4$. The latter differs from the values obtained by first-principles calculations. The derived Fermi temperature $T_F \cong 20,000\ K$ for BiH$_4$ positions this molecular hydride between the unconventional and conventional superconductors bands in the

Uemura plot. This position is outside of the band where covalently bonded and clathrate hydrides are located. The ratio $\Theta_D/T_F = 0.026$ of BiH4 is typical for pure metals and A-15 alloys. This implies that the BiH4, is the first hydride superconductor which complains with the Migdal's theorem.

The compliance of the molecular hydride superconductor BiH$_4$ with the Migdal's theorem

I. Introduction.

The discovery of a superconducting state in pressurized H$_3$S [1] with a transition temperature $T_c = 203\ K$ represented the triumph of modern experimental and theoretical physics. During the decade following this discovery, about six hundreds of new hydride phases were discovered during experimental quests and first-principles calculations [2–35]. The current progress in the field has been reviewed [36–41]. During the last decade, several important questions on fundamental properties of highly compressed and ambient pressure superconductors have been discussed [42–53].

There are two dominant classes of superhydrides that are primarily studied. The first class is the compounds with covalently bonded hydrogen. Historically, this class of high-T_c hydrides was first discovered experimentally [54,55].

The second class is the clathrate hydrides, where there are several sign superconducting phases, for instance, LaH$_{10}$ [4–6,56], YH$_6$ [8,56,57], CaH$_6$ [58,59], and some ternary and quarterly hydrides.

However, both of these classes of hydrides share a common feature - a three-dimensional sublattice formed by dissociated hydrogen ions, which implies that the molecular form of hydrogen in these compounds has dissociated. While hydrogen molecules have an H–H distance of 74 pm, these three-dimensional metallic conducting sublattices in covalently bonded and clathrate hydrides exhibit much larger H–H distance (151 pm in H$_3$S and 115 pm in LaH$_{10}$. [60]).

It should be noted, that the hydrogen in metals is the topic for studies for more than 150 years [61], about a hundred years ago, it was found that atomic hydrogen does not react with pure bismuth [62]. Despite a fact that the electronegativity χ (and, thus, chemical properties) of the metals at high pressure are radically different from the ones at normal conditions [63] (for instance, elemental bismuth is changing its electronegativity from $\chi(P = 0\ GPa) = 1.2$ to

$\chi(P = 200\ GPa) = -5.2$ [63]) we should not exclude that atomic hydrogen can occupy some interstitial sites in the crystal lattice at high pressures, similar to the occupation of interstitial sites in alloys [64] at ambient pressure. Hydrogen atoms vibrate mainly with localized (optical) modes at their interstitial sites [65], and, in addition, at the modes associated with strongly distorted (by the presence of the hydrogen) lattice vibrations (which are short-wavelength acoustic modes of the distorted lattice [65]). All mentioned above reasons cause the change in the phonon spectrum, and as a consequence of it, the electron-phonon coupling constant λ_{e-ph} might also enhance.

From other hand, theoretical studies, including first-principles calculations (fpc), have predicted [66,67] that to achieve metallic conductivity and a superconducting state at liquid nitrogen temperatures in compressed hydrogen, the formation of a sublattice of dissociated molecular hydrogen is not strictly necessary.

And recently, a third class of highly compressed superconducting hydrides has been experimentally discovered, in which hydrogen retains its molecular form but exhibits metallization when compressed in the megabar range [68,69]. This class is currently represented by two superhydrides, BaH_{12} and BiH_4, which both exhibit the smallest H-H distance of 81 pm in the pressure ranges [69], where the highest T_c is achieved for each compound.

The first-principles study of the phase diagram and superconductivity in Bi-H system was performed by Ma *et al* [70] in 2015. And to the best of our knowledge Shan *et al.* [69] performed first experimental study of this system.

Here we have analysed the currently available experimental data for the BaH_{12} [68] and BiH_4 [69] molecular hydrides.

II. Utilized models

There is no direct microscopy with submicron resolution, which can be used to reveal structural parameters of highly compressed materials in the diamond anvil cell (DAC). In attempt to resolve this problem, in [71,72] we proposed to use the Williamson-Hall (WH) analysis[73] of the X-ray diffraction (XRD) data:

$$\beta(\theta, P) = \frac{k_s \times \lambda_{X-ray}}{D(P) \times cos(\theta)} + 4 \times \varepsilon(P) \times tan(\theta), \tag{1}$$

where $\beta(\theta, P)$ is integral breadth of the peak in experimental XRD scan, k_s is the Scherrer constant usually assigned as 0.9 [74–77], λ_{X-ray} is the wavelength of the radiation, $D(P)$ is the mean size of coherent scattering regions, and the $\varepsilon(P)$ is the mean microstrain in crystalline lattice. Experimental XRD scans for BaH$_{12}$ hydride were kindly provided by the authors [68]. We processed these datasets by the DIOPTAS software [78].

One of the primary parameters of any electron-phonon superconductors is the Debye temperature Θ_D which can be deduced from the fit of measured thermal dependence of normal state resistance $R(T)$ to the Bloch- Grüneisen (BG) equation [79,80]:

$$R(T) = R_0 + A\left(\frac{T}{\Theta_D}\right)^5 \int_0^{\frac{\Theta_D}{T}} \frac{x^5}{(e^x-1)(1-e^{-x})} dx \tag{2}$$

where where R_0, A, and Θ_D are free-fitting parameters. Deduced Θ_D and measured in experiment T_c can be used to deduce the electron-phonon coupling constant λ_{e-ph} as a root of the system of McMillan equations [81,82] :

$$T_c = \frac{\Theta_D}{1.4} e^{\left[-\frac{1.04\left(1+\lambda_{e-ph}\right)}{\lambda_{e-ph}-\mu^*\left(1+0.62\lambda_{e-ph}\right)}\right]} \cdot f_1 \cdot f_2^* \tag{3}$$

$$f_1 = \left(1 + \left(\frac{\lambda_{e-ph}}{2.46(1+3.8\mu^*)}\right)^{3/2}\right)^{1/3} \tag{4}$$

$$f_2^* = 1 + (0.0241 - 0.0735 \cdot \mu^*) \cdot \lambda_{e-ph}^2 \tag{5}$$

where μ^* is the Coulomb pseudopotential ($\mu^* = 0.10 - 0.16$ [7,9]) for which we used the mean value of $\mu^* = 0.13$ below. Derived λ_{e-ph} can be compared with the value calculated by the first principles calculations.

Recently, Pinsook and Tanthum [83] proposed that experimental $R(T)$ can be fitted to the equation based on the Einstein temperature, Θ_E:

$$R(T) = R_0 + A \cdot \frac{\frac{\Theta_E^2}{T}}{\left(e^{\frac{\Theta_E}{T}}-1\right)\left(1-e^{-\frac{\Theta_E}{T}}\right)} \tag{6}$$

where R_0, A, and Θ_E are free-fitting parameters. Pinsook and Tanthum [83] found that the deduced Θ_E is approximately equal to the temperature $\left(\frac{\hbar}{k_B}\omega_{ln}\right)$ associated with the logarithmically averaged characteristic frequency ω_{ln} in the Allen-Dynes approximation [84,85] of the Eliashberg theory of electron-phonon superconductivity [86]:

$$T_c = \frac{1}{1.20}\left(\frac{\hbar}{k_B}\omega_{ln}\right)e^{\left[-\frac{1.04\left(1+\lambda_{e-ph}\right)}{\lambda_{e-ph}-\mu^*\left(1+0.62\lambda_{e-ph}\right)}\right]} \cdot f_1 \cdot f_2 \tag{7}$$

$$f_1 = \left(1 + \left(\frac{\lambda_{e-ph}}{2.46(1+3.8\mu^*)}\right)^{3/2}\right)^{1/3} \tag{8}$$

$$f_2 = 1 + \frac{\left(\frac{\langle\omega^2\rangle^{1/2}}{\omega_{ln}}-1\right)\lambda_{e-ph}^2}{\lambda_{e-ph}^2+\left(1.82(1+6.3\mu^*)\left(\frac{\langle\omega^2\rangle^{1/2}}{\omega_{ln}}\right)\right)^2} \tag{9}$$

$$\langle\omega^2\rangle^{1/2} = \frac{2}{\lambda_{e-ph}}\int_0^\infty \omega \times \alpha^2 \times F(\omega)d\omega \tag{10}$$

In [82,87] we proposed to replace Eqs. 8,9 by approximated Eq. 5, because the values of $\alpha^2 \times F(\omega)$ and ω_{ln} can not be deduced from experimental $R(T)$ datasets. Thus, we also used the following equation:

$$T_c = \frac{\Theta_E}{1.20}e^{\left[-\frac{1.04\left(1+\lambda_{e-ph,E}\right)}{\lambda_{e-ph}-\mu^*\left(1+0.62\lambda_{e-ph,E}\right)}\right]} \cdot f_1 \cdot f_2^* \tag{11}$$

for the independent determination of the electron-phonon coupling constant, $\lambda_{e-ph,E}$, from the deduced Einstein temperature, Θ_E.

In this work we derived the ground state superconducting coherence length $\xi(0)$ from the fit of the upper critical field data $B_{c2}(T)$ dataset to the single-band analytical approximation[88] for the Helfand-Werthamer theory [89]:

$$B_{c2}(T) = \frac{\phi_0}{2\pi\xi^2(0)} \times \left(\frac{1-\left(\frac{T}{T_c}\right)^2}{1+0.42\times\left(\frac{T}{T_c}\right)^{1.47}} \right) \tag{12}$$

where ϕ_0 is the superconducting flux quantum.

III. Parameters of the BaH$_{12}$ phase

To determine the instrumental broadening of the XRD machine used in [68], we analyzed XRD scan for calibrated CeO$_2$, which was kindly provided to us by D. Semenok [68]. Data for CeO$_2$ was procced by DIOPTAS [78] software. XRD peaks were fitted to the sum of gaussians:

$$I(2\theta) = A_{bg} + \sum_{k=1}^{N} \frac{A_k}{w\sqrt{\frac{\pi}{2}}} \times e^{-2\frac{\left(2\theta-2\theta_{peak,k}\right)^2}{w^2}}, \tag{13}$$

where A_k is the peak area, $2\theta_{peak,k}$ is the peak position, $\beta_k(2\theta) = w\sqrt{\frac{\pi}{2}}$ is peak integral breadth, and A_k, $2\theta_{peak,k}$, and w are-free fitting parameters. The background level, A_{bg}, was a manually adjusted parameter in each XRD fit in the DIOPTAS software [78] and it was a free fitting parameter in final fit in Origin software [90].

Derived peaks breadth, $\beta_i(2\theta)$, were fitted to Caglioti equation [91]:

$$\beta_{inst}(2\theta) = \sqrt{U \cdot tan^2\left(\frac{2\theta}{2}\right) + V \cdot tan\left(\frac{2\theta}{2}\right) + W}, \tag{14}$$

where U, V, and W are free-fitting parameters. Result of the fit is shown in Fig. 1, where derived parameters are: $U = 0$, $V = 0$, $W = (1.29 \pm 0.06) \times 10^{-6}$.
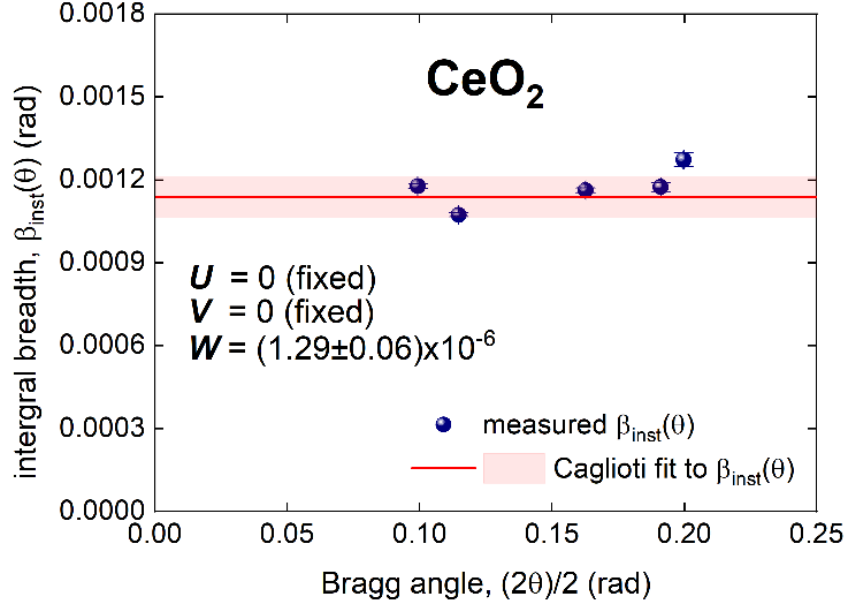
Figure 1. Experimental $\beta_i(\theta)$ data for standard CeO₂ sample. Raw XRD scan was provided by D. Semenok. 95% confidence bands are shown by pink shadow area.

Peaks in XRD scans of BaH₁₂ were fitted to Eq. 13 and $\beta_{measured}(2\theta)$ datasets were deduced. The peaks breadth originated from the BaH₁₂ phase, $\beta_{BaH12}(2\theta)$, were calculated by the equation:

$$\beta_{BaH12}(2\theta) = \sqrt{\beta_{measured}^2(2\theta) - \beta_{inst}^2(2\theta)}, \tag{15}$$

Derived $\beta_{BaH12}(\theta, P)$ datasets were fitted to the WH equation (Eq. 1). Deduced values from these fits, $D(P)$ and $\varepsilon(P)$, are shown in Fig. 2.

One can see (Fig. 2) that $D(P)$ and $\varepsilon(P)$ are practically independent from applied pressure in the studied range of $126\ GPa \leq P \leq 160\ GPa$. It is interesting to note, that highly compressed BaH₁₂ has negligible level of micro-strain.
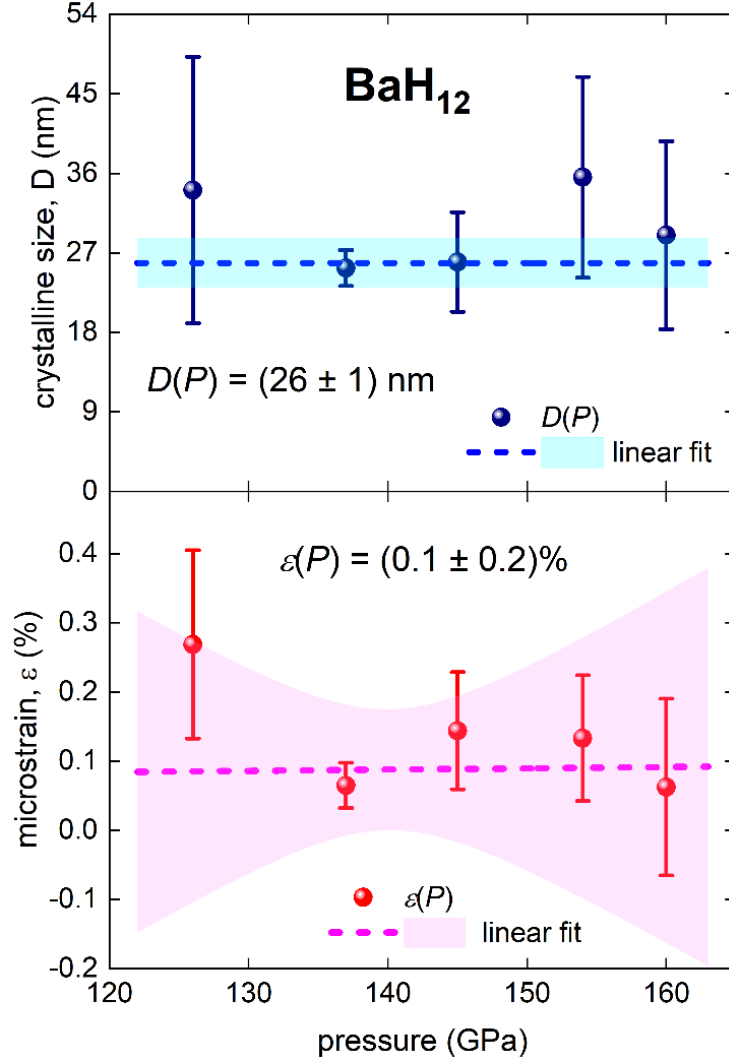
Figure 2. Derived (a) grain size $D(P)$ and (b) micro-strain $\varepsilon(P)$ in highly compressed BaH$_{12}$. Raw XRD data was measured by Chen *et al.* [68]. 95% confidence bands are shown by (a) cyan and (b) magenta shadow areas.

In Figures 3 and 4, we showed the $R(T, P = 100\ GPa)$ data measured in BaH$_{12}$ by Chen *et al.* [68] and data fits to Bloch-Grüneisen (Eq. 2) and Einstein (Eq. 6) models in panels *a* and *b*, respectively. The substitution derived Θ_D and Θ_E in respectful equations returns the $\lambda_{e-ph,D}$ and $\lambda_{e-ph,E}$ values which appear to be practical equal to each other $\lambda_{e-ph,E} = \lambda_{e-ph,D} \cong 0.71$ (Fig. 3), and $\lambda_{e-ph,E} = 0.70 \cong \lambda_{e-ph,D} = 0.69$ (Fig. 4). We also found that $\Theta_E/\Theta_D \cong 0.805$ (Figs. 3,4), which is lower than the theoretical value of $\Theta_E/\Theta_D = 0.828$. It should be noted that the

obtained $\Theta_E/\Theta_D \cong 0.805$ value is very close to the one deduced for highly compressed

LaB$_2$H$_8$[87].
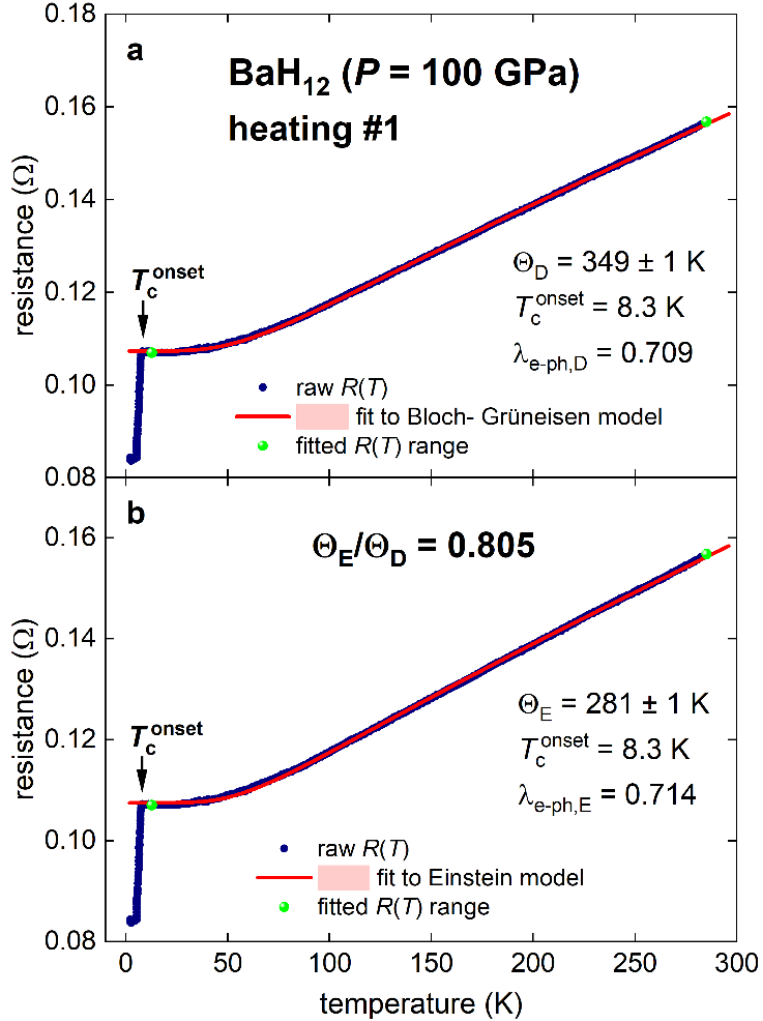
Figure 3. $R(T, P = 100\ GPa)$ dataset for BaH$_{12}$ (heating #1) and data fit to (**a**) Bloch-Grüneisen (Eq. 2) and (**b**) Einstein (Eq. 6) models. Raw $R(T, P = 100\ GPa)$ data reported by Chen *et al.* [68]. Derived parameters are shown in panels (**a**) and (**b**). Goodness of fit: (**a**) $R = 0.9998$ and (**b**) $R = 0.9997$. 95% confidence bands are shown by pink shadow areas.

Moreover, the derived values of $\lambda_{e-ph}(P = 100\ GPa) \cong 0.70$ differs from the value

$\lambda_{e-ph}(P = 140\ GPa) = 0.95$ obtained by first principles calculations [68]. Such a difference can

originate from the difference in pressure used in experiment ($P = 100\ GPa$) and the one used

for calculations ($P = 140\ GPa$). Another probable reason is the presence of vacancies in the

crystalline structure of BaH$_{12}$. Atomic-scale vacancies are now considered an important structural defect that can determine T_c in high-pressure superconductors [35,92].
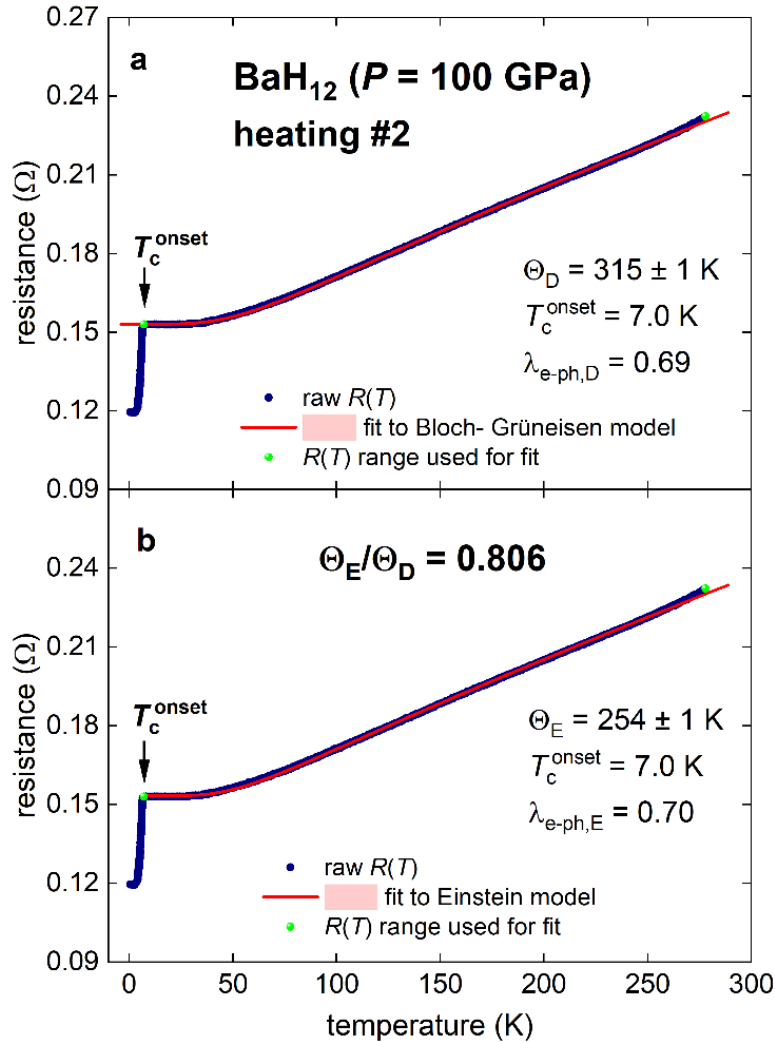
Figure 4. $R(T, P = 100\ GPa)$ dataset for BaH$_{12}$ (heating #2) and data fit to (**a**) Bloch-Grüneisen (Eq. 2) and (**b**) Einstein (Eq. 6) models. Raw $R(T, P = 100\ GPa)$ data reported by Chen *et al*. [68]. Derived parameters are shown in panels (**a**) and (**b**). Goodness of fit: (**a**) $R = 0.9998$ and (**b**) $R = 0.9997$. 95% confidence bands are shown by pink shadow areas.

IV. Parameters of the BiH₄ phase

In Figure 5, we showed the $R(T, P = 172\ GPa)$ data measured in BiH₄ hydride by Shan *et al*.[69]. Data fits to Bloch-Grüneisen (Eq. 2) and Einstein (Eq. 6) models are shown in panels **a** and **b** of Fig. 5, respectively.

To calculate the $\lambda_{e-ph,D}$ and $\lambda_{e-ph,E}$ values we defined the transition temperature by a strict resistance criterion $\frac{R(T=T_C)}{R_{norm}} \rightarrow 0.05$. The substitution of the derived Θ_D and Θ_E in respectful equations returns the $\lambda_{e-ph,D}$ and $\lambda_{e-ph,E}$ values which appear to be equal to each other, $\lambda_{e-ph,E} = \lambda_{e-ph,D} = 2.9$ (Fig. 5), In addition, we found that the ratio $\Theta_E/\Theta_D = 0.822$ (Fig. 5) is practically equal to the theoretical value of $\Theta_E/\Theta_D = 0.828$.
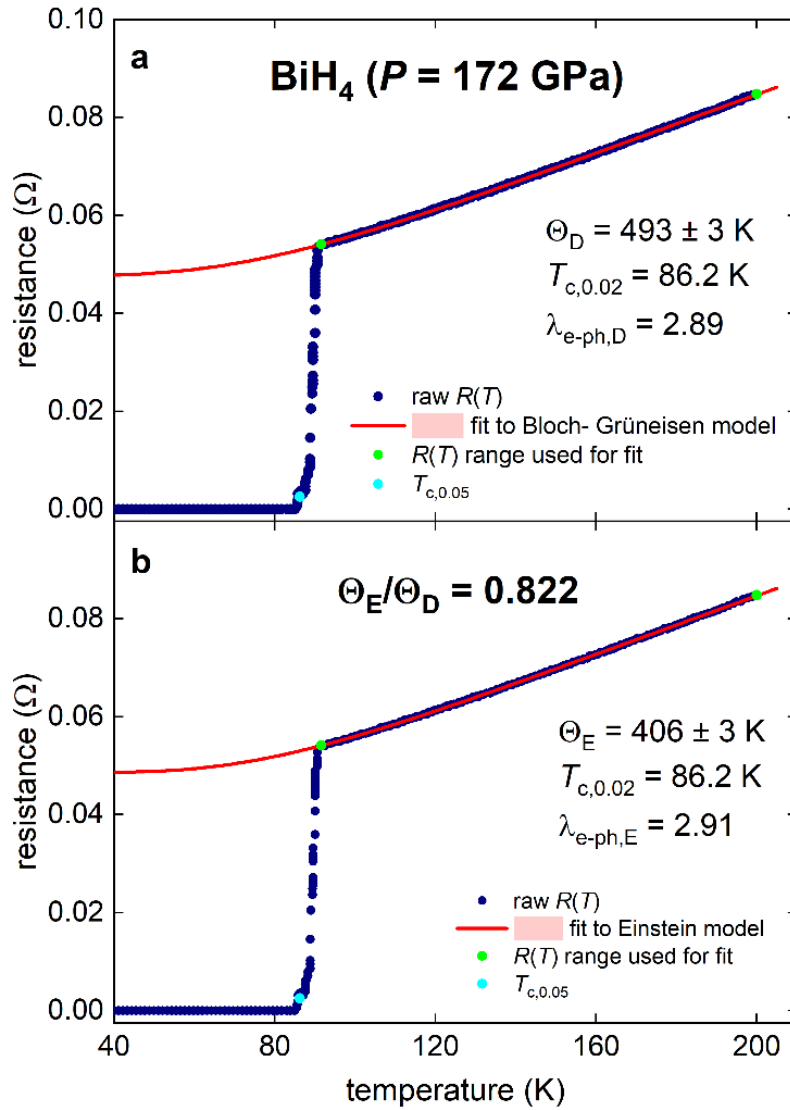
Figure 5. $R(T, P = 172\ GPa)$ dataset for BiH$_4$ and data fit to (**a**) Bloch-Grüneisen (Eq. 2) and (**b**) Einstein (Eq. 6) models. Raw $R(T, P = 100\ GPa)$ data reported by Shan *et al.* [69]. Derived parameters are shown in panels. Goodness of fit is $R = 0.9998$ for both panels. 95% confidence bands are shown by pink shadow areas.

The derived Θ_E/Θ_D values for BaH12 and BiH4 confirm the proposal by Pinsook and Tanthum[83] that the Einstein temperature Θ_E can be used instead of the value $\left(\frac{\hbar}{k_B}\omega_{ln}\right)$ in the Allen-Dynes equation[85].

Considering results of the first-principles calculations by Ma *et al.* [70], we found that the closest theoretical $\left(\frac{\hbar}{k_B}\omega_{ln}\right)$ value to our value $\Theta_E(P = 172\ GPa) = 406\ K$ (deduced from experimental $R(T)$) is $\left(\frac{\hbar}{k_B}\omega_{ln}\right)(P = 150\ GPa) = 507\ K$ calculated for *P21/m*-BiH2 phase.

Moreover, the deduced $\lambda_{e-ph,E}(172\ GPa) = \lambda_{e-ph,D}(172\ GPa) = 2.9$ is remarkably different from the value calculated by first-principles calculations $\lambda_{e-ph,fpc}(170\ GPa) = 2.01$ [69] and $\lambda_{e-ph,fpc}(150\ GPa) \leq 1.34$ for BiH$_n$ (*n* = 2,3,4,5,6).

Such a large difference between the deduced λ_{e-ph} from experimental $R(T)$ (by utilizing two approaches Eqs. 2-11) and the calculated values by first-principles has not been reported before [83,93]. Instead, it was shown a reasonable agreement between experimental and calculated values [83,93]. Based on this, we can state that the deduced value of $\lambda_{e-ph}(172\ GPa) = 2.9$ is correct.

Such a large difference should be commented. Our current interpretation of this difference is based on idea that some small part of the molecular hydrogen is actually dissociated at such high pressure of $P = 172\ GPa$. The possibility of partial dissociation of molecular hydrogen cannot be excluded, based on available literature which we reviewed in the *Introduction* part. If so, the dissociated hydrogen makes contribution in the phonon spectrum. This contribution distorts the phonon spectrum, and, perhaps, creates new bands in addition to the bands calculated to the date [69,70] in BiH4. In the result, the λ_{e-ph} value can be enhanced in comparison with the $\lambda_{e-ph,fpc}$ value, which is calculated based on the assumption that the real structure of the BiH4 is formed by bismuth and molecular hydrogen only[69,70].

In Figure 6, we showed the upper critical field $B_{c2}(T)$ which was deduced from the $R(T, B, P = 172\ GPa)$ data reported by Shan et al.[69]. For the derivation, we used the resistive criterion of $\frac{R(T=T_c)}{R_{norm}} \to 0.07$.
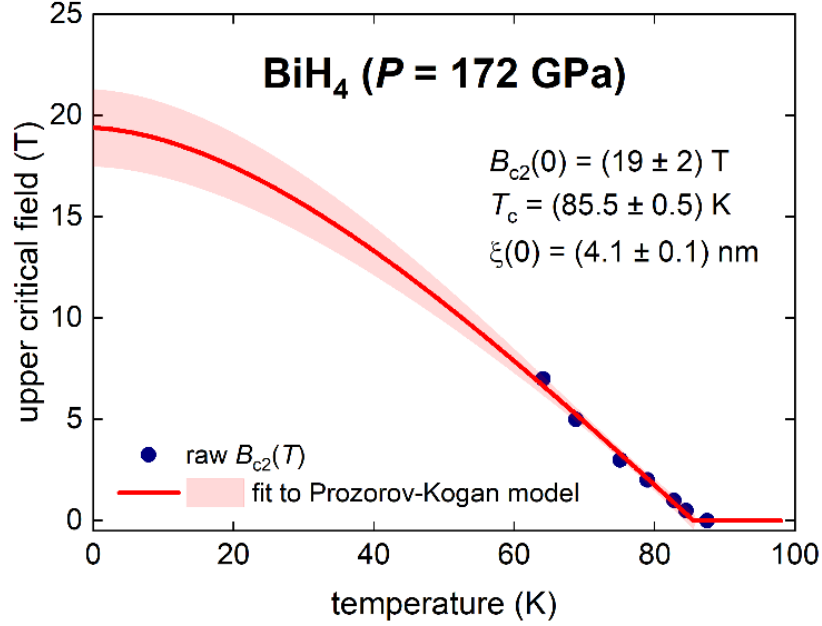
Figure 6. $B_{c2}(T)$ for BiH₄ and data fit Eq. 12. Raw $R(T, B, P = 172\ GPa)$ data reported by Shan et al.[69] $B_{c2}(T)$ datasets were derived by applying criterion $\frac{R(T=T_c)}{R_{norm}} = 0.07$. 95% confidence intervals are indicated by the pink shaded area.

The ground state coherence length, $\xi(0) = 4.1 \pm 0.1\ nm$ was deduced from the $B_{c2}(T)$ fit to the Equation 12 (Figure 6). The deduced value was substituted in the Equation 11 to calculate the Fermi temperature:

$$T_F = \frac{\pi^2 m_e}{8 \cdot k_B} \cdot \left(1 + \lambda_{e-ph}\right) \cdot \xi^2(0) \cdot \left(\frac{\alpha k_B T_c}{\hbar}\right)^2, \tag{16}$$

where m_e is bare electron mass, $\hbar$ is reduced Planck constant, $\alpha = \frac{2\Delta(0)}{k_B T_c}$, and $\lambda_{e-ph} = 2.9$ was taken from Fig. 5. The $\frac{2\Delta(0)}{k_B T_c}$ ratio was calculated by linear approximated relation proposed in Ref.[94]:

$$\alpha \equiv \frac{2\Delta(0)}{k_B T_C} = 3.26 + 0.74 \times \lambda_{e-ph}. \tag{17}$$

Calculated $T_F = 19{,}500\ K$ implies that the BiH_4 falls between the unconventional and conventional superconductors bands in the Uemura plot with $T_c/T_F = 0.0044$ (Fig. 7). This position is outside (towards the BCS superconductivity band) the band where covalently bonded and clathrate hydrides are located (Fig. 7).
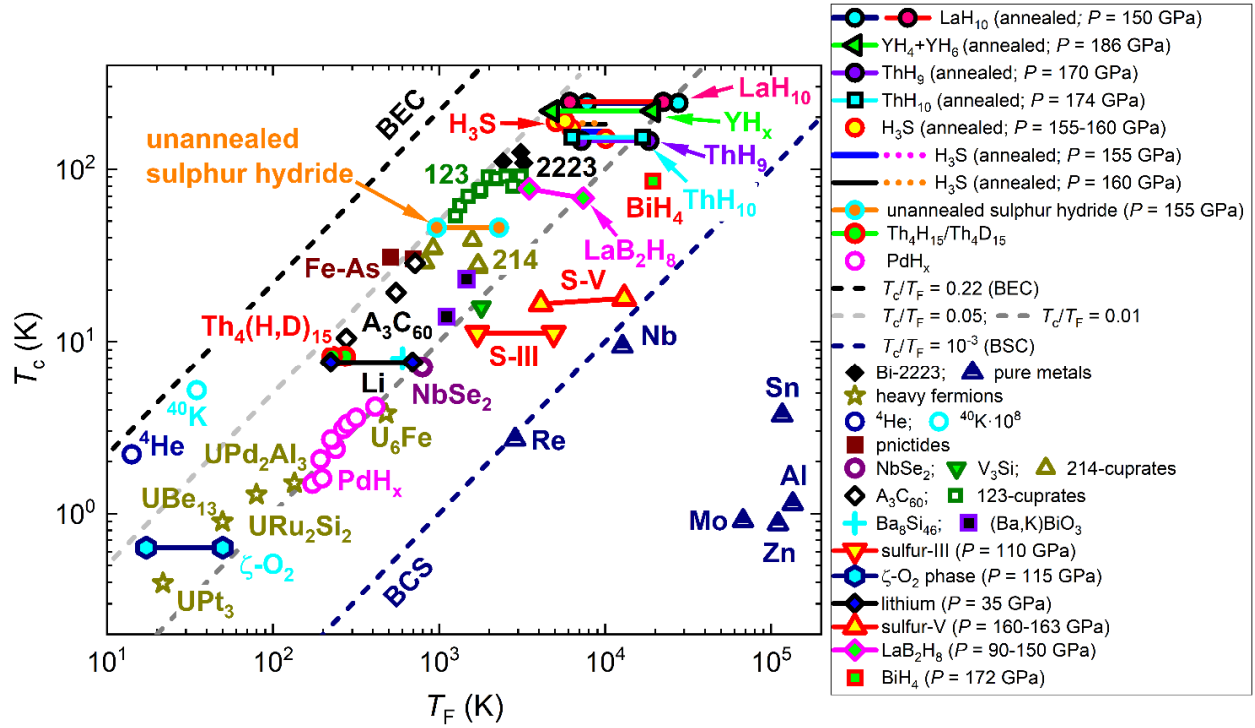
Figure 7. Uemura plot (T_c vs. T_F) where BiH_4 phase is shown together with main superconducting families. References to the original data are in Refs.[72,95–97]. The position of the BiH_4 phase is outside of the band, where other hydrogen-based superconductors are located, and toward the band of classical BCS superconductors.

However, the most important finding in this work is the established ratio of $\Theta_D/T_F = 0.026$ in BiH_4 (Fig. 8). This value is similar to the Θ_D/T_F in pure metals and A-15 alloys (Fig. 8). Thus, the BiH_4 is the first discovered highly compressed high-T_c superhydride [72,93,95,96] which complies [98–103] with the Migdal's theorem [104]. This is unexpected result. Perhaps this result is additional evidence for the presence of the dissociated hydrogen in the structure of highly

compressed BiH4, because the metallization of the dissociated hydrogen should bust the Fermi surface size.
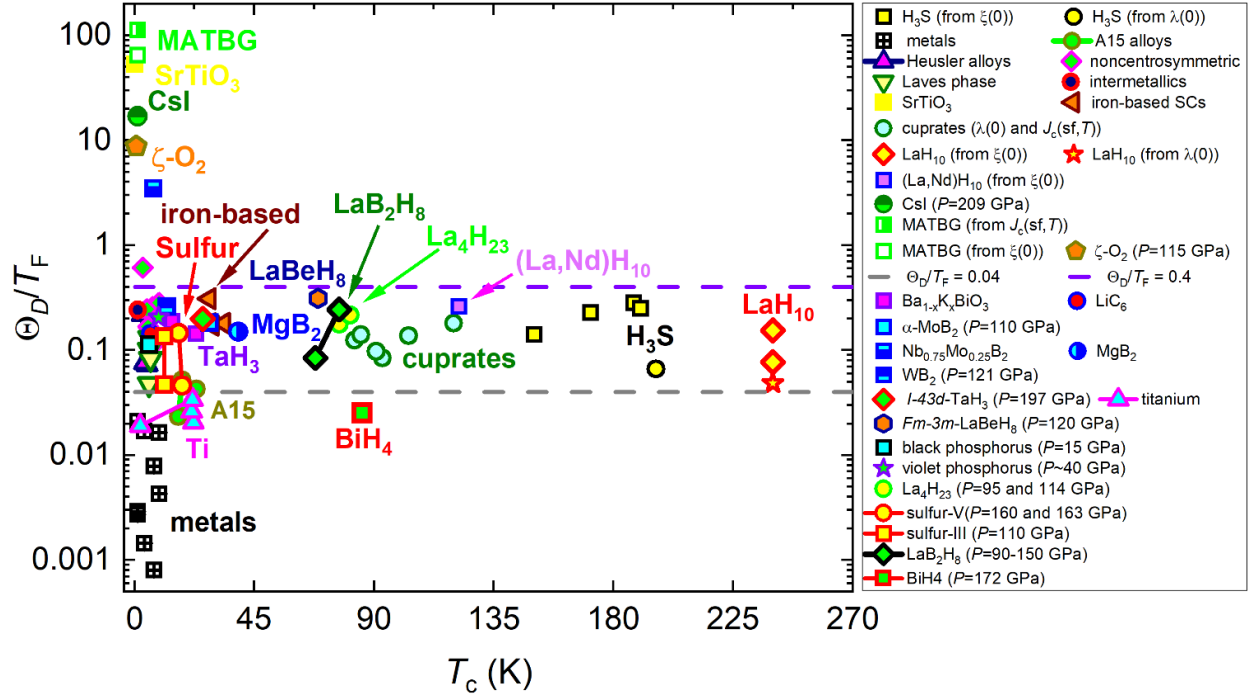
Figure 7. $\frac{\Theta_D}{T_F}$ *vs* T_c plot where BiH4 phase is shown together with main superconducting families. References to the original data are in Refs.[72,93,95,96].

V. Conclusions

In this study, we analysed available experimental data reported for highly compressed molecular hydrides BaH12 [68] and BiH4 [69].

In the result, we confirm that the proposal by Pinsook and Tanthum [83] that the Einstein temperature Θ_E can be used instead of the $\left(\frac{\hbar}{k_B}\omega_{ln}\right)$ term in the Allen-Dynes equation [85].

One of the central findings of our study is that the BiH4 exhibits a low level of nonadiabaticity, $\Theta_D/T_F = 0.026$, and, thus, the BiH4 is the first hydride which complies with Migdal theorem [104].

We have proposed that the BiH$_4$ samples at $P = 172\,GPa$ contain some hydrogen in dissociated metallized state.

Acknowledgements

References

1. Drozdov, A. P., Eremets, M. I., Troyan, I. A., Ksenofontov, V. & Shylin, S. I. Conventional superconductivity at 203 kelvin at high pressures in the sulfur hydride system. *Nature* **525**, 73–76 (2015).
2. Wrona, I. A., Niegodajew, P. & Durajski, A. P. A recipe for an effective selection of promising candidates for high-temperature superconductors among binary hydrides. *Materials Today Physics* **46**, 101499 (2024).
3. Bhattacharyya, P. *et al.* Imaging the Meissner effect in hydride superconductors using quantum sensors. *Nature* **627**, 73–79 (2024).
4. Drozdov, A. P. *et al.* Superconductivity at 250 K in lanthanum hydride under high pressures. *Nature* **569**, 528–531 (2019).
5. Somayazulu, M. *et al.* Evidence for Superconductivity above 260 K in Lanthanum Superhydride at Megabar Pressures. *Phys Rev Lett* **122**, 027001 (2019).
6. Sun, D. *et al.* High-temperature superconductivity on the verge of a structural instability in lanthanum superhydride. *Nat Commun* **12**, 6863 (2021).
7. Chen, W. *et al.* High-Temperature Superconducting Phases in Cerium Superhydride with a Tc up to 115 K below a Pressure of 1 Megabar. *Phys Rev Lett* **127**, 117001 (2021).
8. Kong, P. *et al.* Superconductivity up to 243 K in the yttrium-hydrogen system under high pressure. *Nat Commun* **12**, 5075 (2021).
9. Semenok, D. Computational design of new superconducting materials and their targeted experimental synthesis. *PhD Thesis; Skolkovo Institute of Science and Technology* (2023) doi:10.13140/RG.2.2.28212.12161.
10. Song, Y. *et al.* Stoichiometric Ternary Superhydride LaBeH8 as a New Template for High-Temperature Superconductivity at 110 K under 80 GPa. *Phys Rev Lett* **130**, 266001 (2023).
11. Chen, W. *et al.* Enhancement of superconducting properties in the La–Ce–H system at moderate pressures. *Nat Commun* **14**, 2660 (2023).
12. Semenok, D. V. *et al.* Effect of Magnetic Impurities on Superconductivity in LaH10. *Advanced Materials* **34**, 2204038 (2022).
13. Chen, L.-C. *et al.* Synthesis and superconductivity in yttrium-cerium hydrides at high pressures. *Nat Commun* **15**, 1809 (2024).

14. Zhang, K. *et al.* High-pressure synthesis of a ternary yttrium-sulfur hydride superconductor with a high Tc of approximately 235 K. *Sci China Phys Mech Astron* **67**, 238211 (2024).

15. Cai, W. *et al.* Superconductivity above 180 K in Ca-Mg Ternary Superhydrides at Megabar Pressures. (2023) doi:10.48550/arXiv.2312.06090.

16. Song, P. *et al.* $(La,Th)H_{10}$: Potential High- T_c (242 K) Superconductors Stabilized Thermodynamically below 200 GPa. *The Journal of Physical Chemistry C* **128**, 2656–2665 (2024).

17. He, X. *et al.* Superconductivity discovered in niobium polyhydride at high pressures. *Materials Today Physics* **40**, 101298 (2024).

18. Song, X. *et al.* Superconductivity above 105 K in Nonclathrate Ternary Lanthanum Borohydride below Megabar Pressure. *J Am Chem Soc* **146**, 13797–13804 (2024).

19. Errea, I. *et al.* Quantum hydrogen-bond symmetrization in the superconducting hydrogen sulfide system. *Nature* **532**, 81–84 (2016).

20. Chen, H., Wang, H. & Shi, J. Enhancing superconducting transition temperature of lanthanum superhydride by increasing hydrogen vacancy concentration. (2024).

21. Nakao, H. *et al.* Superconductivity of Pure H_3S Synthesized from Elemental Sulfur and Hydrogen. *J Physical Soc Japan* **88**, 123701 (2019).

22. Laniel, D. *et al.* High-pressure synthesis of seven lanthanum hydrides with a significant variability of hydrogen content. *Nat Commun* **13**, 6987 (2022).

23. Salke, N. P. *et al.* Synthesis of clathrate cerium superhydride CeH9 at 80-100 GPa with atomic hydrogen sublattice. *Nat Commun* **10**, 4453 (2019).

24. Gao, K. *et al.* Prediction of high- T_c superconductivity in ternary actinium beryllium hydrides at low pressure. *Phys Rev B* **109**, 014501 (2024).

25. Huang, G. *et al.* Synthesis of superconducting phase of $La_{0.5}Ce_{0.5}H_{10}$ at high pressures. *Journal of Physics: Condensed Matter* **36**, 075702 (2024).

26. Cao, Z.-Y. *et al.* Probing superconducting gap in CeH$_9$ under pressure. (2024) doi:10.48550/arXiv.2401.12682.

27. Liu, H., Liu, C., Ma, Y. & Chen, C. Prominent stress-driven anomalies in superconductivity of yttrium hexahydride. *Phys Rev B* **109**, 064513 (2024).

28. Chen, S. *et al.* Superior Superconducting Properties Realized in Quaternary La–Y–Ce Hydrides at Moderate Pressures. *J Am Chem Soc* **146**, 14105–14113 (2024).

29. Guo, J. *et al.* Unusual metallic state in superconducting A15-type La4H23. *Natl Sci Rev* (2024) doi:10.1093/nsr/nwae149.

30. Chen, S. *et al.* Synthesis and superconductivity in $(La,Ca)H_{10}$ under high pressure. *Phys Rev B* **109**, 224510 (2024).

31. Ma, C. *et al.* Synthesis of medium-entropy alloy superhydride $(La,Y,Ce)H_{10\pm x}$ with high-temperature superconductivity under high pressure. *Phys Rev B* **111**, 024505 (2025).

32. Zhao, W. *et al.* High temperature superconductivity of quaternary hydrides XM3Be4H32 (X, M = Ca, Sr, Ba, Y, La, Ac, Th) under moderate pressure. *Materials Today Physics* **43**, 101387 (2024).

33. Purans, J. *et al.* Local electronic structure rearrangements and strong anharmonicity in YH3 under pressures up to 180 GPa. *Nat Commun* **12**, 1765 (2021).

34. Zhang, K. *et al.* Synthesis and Superconductivity of Ternary A15-(Lu, Y) $_4$ H $_{23}$ at High Pressures. *J Am Chem Soc* **147**, 11879–11885 (2025).

35. Ma, C. *et al.* Hydrogen-Vacancy-Induced Stable Superconducting Niobium Hydride at High Pressure. *J Am Chem Soc* **147**, 11028–11035 (2025).

36. Bondarenko, S. I., Timofeev, V. P., Koverya, V. P. & Krevsun, A. V. Hydrogen in superconductors. (2024).

37. Eremets, M. I. The current status and future development of high-temperature conventional superconductivity. *Natl Sci Rev* (2024) doi:10.1093/nsr/nwae047.

38. Lilia, B. *et al.* The 2021 room-temperature superconductivity roadmap. *Journal of Physics: Condensed Matter* **34**, 183002 (2022).

39. Troyan, I. A., Semenok, D. V., Sadakov, A. V., Lyubutin, I. . S. & Pudalov, V. M. PROGRESS, PROBLEMY I PERSPEKTIVY KOMNATNO-TEMPERATURNOY SVERKhPROVODIMOSTI. *Žurnal èksperimental'noj i teoretičeskoj fiziki* **166**, 74–88 (2024).

40. Troyan, I. A. *et al.* High-temperature superconductivity in hydrides. *Physics-Uspekhi* **65**, 748–761 (2022).

41. Eremets, M. I. *et al.* High-Temperature Superconductivity in Hydrides: Experimental Evidence and Details. *J Supercond Nov Magn* **35**, 965–977 (2022).

42. Tallon, J. L. Flux-trapping experiments on ultra-high pressure hydrides as evidence of superconductivity. (2024).

43. Prozorov, R. On the trapped magnetic moment in type-II superconductors. (2024).

44. Ho, K. O. & Yang, S. Quantum sensor settles debate about superconductivity in hydrides. *Nature* (2024) doi:10.1038/d41586-024-00423-y.

45. Goh, S. K., Zhang, W. & Yip, K. Y. Trapped magnetic flux in superconducting hydrides. *Nat Phys* (2023) doi:10.1038/s41567-023-02101-8.

46. Balakirev, F. F., Minkov, V. S., Drozdov, A. P. & Eremets, M. I. Evidence of Superconductivity in Electrical Resistance Measurements of Hydrides Under High Pressure. *J Supercond Nov Magn* (2024) doi:10.1007/s10948-024-06792-9.

47. Talantsev, E. F., Minkov, V. S., Balakirev, F. F. & Eremets, M. I. Comment on "Nonstandard superconductivity or no superconductivity in hydrides under high pressure". *Phys Rev B* **110**, 186501 (2024).

48. Mark, A. C. & Hemley, R. J. On the Lineshapes of Temperature-Dependent Transport Measurements of Superconductors Under Pressure. *J Supercond Nov Magn* **38**, 25 (2025).

49. Gao, K. *et al.* The Maximum T_c of Conventional Superconductors at Ambient Pressure. (2025).

50. Cao, Z.-Y. *et al.* Probing superconducting gap in CeH_9 under pressure. *ArXiv* (2024).

51. Cerqueira, T. F. T., Fang, Y.-W., Errea, I., Sanna, A. & Marques, M. A. L. Searching Materials Space for Hydride Superconductors at Ambient Pressure. *ArXiv* (2024).

52. Pickard, C. J., Errea, I. & Eremets, M. I. Superconducting Hydrides Under Pressure. *Annu Rev Condens Matter Phys* **11**, 57–76 (2020).

53. Sadovskii, M. V. Limits of Eliashberg theory and bounds for superconducting transition temperature. *Physics-Uspekhi* **65**, 724–739 (2022).

54. Drozdov, A. P., Eremets, M. I. & Troyan, I. A. Conventional superconductivity at 190 K at high pressures. (2014).

55. Drozdov, A. P., Eremets, M. I. & Troyan, I. A. Superconductivity above 100 K in PH3 at high pressures. (2015).

56. Liu, H., Naumov, I. I., Hoffmann, R., Ashcroft, N. W. & Hemley, R. J. Potential high-T_c superconducting lanthanum and yttrium hydrides at high pressure. *Proceedings of the National Academy of Sciences* **114**, 6990–6995 (2017).

57. Troyan, I. A. *et al.* Anomalous High-Temperature Superconductivity in YH_6. *Advanced Materials* **33**, 2006832 (2021).

58. Wang, H., Tse, J. S., Tanaka, K., Iitaka, T. & Ma, Y. Superconductive sodalite-like clathrate calcium hydride at high pressures. *Proceedings of the National Academy of Sciences* **109**, 6463–6466 (2012).

59. Ma, L. *et al.* High-Temperature Superconducting Phase in Clathrate Calcium Hydride CaH6 up to 215 K at a Pressure of 172 GPa. *Phys Rev Lett* **128**, 167001 (2022).

60. Shan, P. *et al.* Molecular Hydride Superconductor BiH_4 with T_c up to 91 K at 170 GPa. *J Am Chem Soc* **147**, 4375–4381 (2025).

61. Johnson, W. H. II. On some remarkable changes produced in iron and steel by the action of hydrogen and acids. *Proceedings of the Royal Society of London* **23**, 168–179 (1875).

62. The behaviour of metals, particularly lead and bismuth, in atomic hydrogen, and attempts to prepare atomic hydrogen from hydrides. *Proceedings of the Royal Society of London. Series A, Containing Papers of a Mathematical and Physical Character* **142**, 275–285 (1933).

63. Dong, X., Oganov, A. R., Cui, H., Zhou, X.-F. & Wang, H.-T. Electronegativity and chemical hardness of elements under pressure. *Proceedings of the National Academy of Sciences* **119**, (2022).

64. Mushnikov, N. V., Gaviko, V. S., Korolyov, A. V. & Zajkov, N. K. Hydrogen-induced magnetic anisotropy and crystal lattice distortion in Sm1−xTbx(Fe0.2Co0.8)2 compounds. *J Alloys Compd* **218**, 165–172 (1995).

65. Schober, H. R. & Stoneham, A. M. Diffusion of hydrogen in transition metals. *Journal of the Less Common Metals* **172–174**, 538–547 (1991).

66. Dogan, M., Oh, S. & Cohen, M. L. High temperature superconductivity in the candidate phases of solid hydrogen. *Journal of Physics: Condensed Matter* **34**, 15LT01 (2022).

67. Dogan, M., Chelikowsky, J. R. & Cohen, M. L. Anisotropy and isotope effect in superconducting solid hydrogen. *Journal of Physics: Condensed Matter* **36**, 01LT01 (2024).

68. Chen, W. *et al.* Synthesis of molecular metallic barium superhydride: pseudocubic BaH12. *Nat Commun* **12**, 1–9 (2021).

69. Shan, P. *et al.* Molecular Hydride Superconductor BiH $_4$ with T_c up to 91 K at 170 GPa. *J Am Chem Soc* **147**, 4375–4381 (2025).

70. Ma, Y. *et al.* High-pressure structures and superconductivity of bismuth hydrides. (2015).

71. Talantsev, E. F. & Chistyakov, V. V. Debye temperature, electron-phonon coupling constant, and three-dome shape of crystalline strain as a function of pressure in highly compressed La$_3$Ni$_2$O$_{7-\delta}$. (2024) doi:10.48612/letters/2024-3-262-268.

72. Talantsev, E. F. & Chistyakov, V. V. The A-15-type superconducting hydride La $_4$ H $_{23}$: a nanograined structure with low strain, strong electron-phonon interaction, and a moderate level of nonadiabaticity. *Supercond Sci Technol* **37**, 095016 (2024).

73. Williamson, G. K. & Hall, W. H. X-ray line broadening from filed aluminium and wolfram. *Acta Metallurgica* **1**, 22–31 (1953).

74. Basak, M., Rahman, Md. L., Ahmed, Md. F., Biswas, B. & Sharmin, N. The use of X-ray diffraction peak profile analysis to determine the structural parameters of cobalt ferrite nanoparticles using Debye-Scherrer, Williamson-Hall, Halder-Wagner and Size-strain plot: Different precipitating agent approach. *J Alloys Compd* **895**, 162694 (2022).

75. Klug, H. P. & Alexander, L. E. *X-Ray Diffraction Procedures: For Polycrystalline and Amorphous Materials*. (Wiley, 1974).

76. Miyajima, Y., Okubo, S., Miyazawa, T., Adachi, H. & Fujii, T. In-situ X-ray diffraction during tensile deformation of ultrafine-grained copper using synchrotron radiation. *Philos Mag Lett* **96**, 294–304 (2016).

77. Balzar, D. X-ray diffraction line broadening: modeling and applications to high-Tc superconductors. *J Res Natl Inst Stand Technol* **98**, 321 (1993).

78. Prescher, C. & Prakapenka, V. B. *DIOPTAS* : a program for reduction of two-dimensional X-ray diffraction data and data exploration. *High Press Res* **35**, 223–230 (2015).

79. Bloch, F. Zum elektrischen Widerstandsgesetz bei tiefen Temperaturen. *Zeitschrift f�r Physik* **59**, 208–214 (1930).

80. Grüneisen, E. Die Abhängigkeit des elektrischen Widerstandes reiner Metalle von der Temperatur. *Ann Phys* **408**, 530–540 (1933).

81. McMillan, W. L. Transition Temperature of Strong-Coupled Superconductors. *Physical Review* **167**, 331–344 (1968).

82. Talantsev, E. F. Advanced McMillan's equation and its application for the analysis of highly-compressed superconductors. *Supercond Sci Technol* **33**, 094009 (2020).

83. Pinsook, U. & Tanthum, P. Universal resistivity from electron-phonon interaction based on Einstein model: Application to near-room temperature superconductors. *Next Materials* **6**, 100302 (2025).

84. Dynes, R. C. McMillan's equation and the Tc of superconductors. *Solid State Commun* **10**, 615–618 (1972).

85. Allen, P. B. & Dynes, R. C. Transition temperature of strong-coupled superconductors reanalyzed. *Phys Rev B* **12**, 905–922 (1975).

86. G. M. Eliashberg. Interactions between Electrons and Lattice Vibrations in a Superconductor. *Sov. Phys.– JETP* **11**, 696 (1960).

87. Talantsev, E. F. Primary superconducting parameters of highly compressed nonclathrate ternary hydride LaB2H8. Preprint at https://doi.org/10.2139/ssrn.5160162 (2025).

88. Prozorov, R. & Kogan, V. G. Practically universal representation of the Helfand-Werthamer upper critical field for any transport scattering rate. *Phys Rev Appl* **22**, 064006 (2024).

89. Helfand, E. & Werthamer, N. R. Temperature and Purity Dependence of the Superconducting Critical Field, Hc2. II. *Physical Review* **147**, 288–294 (1966).

90. Seifert, E. OriginPro 9.1: Scientific Data Analysis and Graphing Software—Software Review. *J Chem Inf Model* **54**, 1552–1552 (2014).

91. Caglioti, G., Paoletti, A. & Ricci, F. P. Choice of collimators for a crystal spectrometer for neutron diffraction. *Nuclear Instruments* **3**, 223–228 (1958).

92. Sanna, A., Pellegrini, C., di Cataldo, S., Profeta, G. & Boeri, L. A possible explanation for the high superconducting Tc in bcc Ti at high pressure. (2023).

93. Talantsev, E. F. The electron–phonon coupling constant and the Debye temperature in polyhydrides of thorium, hexadeuteride of yttrium, and metallic hydrogen phase III. *J Appl Phys* **130**, 195901 (2021).

94. Talantsev, E. F. The Compliance of the Upper Critical Field in Magic-Angle Multilayer Graphene with the Pauli Limit. *Materials* **16**, 256 (2022).

95. Talantsev, E. F. Quantifying the Nonadiabaticity Strength Constant in Recently Discovered Highly Compressed Superconductors. *Symmetry (Basel)* **15**, 1632 (2023).

96. Talantsev, E. F. Classifying hydrogen-rich superconductors. *Mater Res Express* **6**, 106002 (2019).

97. Talantsev, E. F. Quantifying Nonadiabaticity in Major Families of Superconductors. *Nanomaterials* **13**, 71 (2022).

98. Cappelluti, E., Grimaldi, C. & Pietronero, L. Electron–phonon driven unconventional superconductivity: The role of small Fermi energies and of nonadiabatic processes. *Physica C: Superconductivity and its Applications* **613**, 1354343 (2023).

99. Pietronero, L., Boeri, L., Cappelluti, E. & Ortenzi, L. Conventional/unconventional superconductivity in high-pressure hydrides and beyond: insights from theory and perspectives. *Quantum Studies: Mathematics and Foundations* **5**, 5–21 (2018).

100. L. Pietronero, L. Boeri, E. Cappellut & L. Ortenzi. Conventional/Unconventional superconductivity in high pressure hydrides and beyond: Insights from theory and perspectives. in *2nd International Workshop 'Towards Room Temperature Superconductivity: Superhydrides and More.' In Recognition of Professor Vitaly Ginzburg.* (eds. Organizers: et al.) (Orange, CA, USA , 2017).

101. Jarlborg, T. & Bianconi, A. Breakdown of the Migdal approximation at Lifshitz transitions with giant zero-point motion in the H3S superconductor. *Sci Rep* **6**, 24816 (2016).

102. Schrodi, F., Oppeneer, P. M. & Aperis, A. Full-bandwidth Eliashberg theory of superconductivity beyond Migdal's approximation. *Phys Rev B* **102**, 024503 (2020).

103. Gor'kov, L. P. Superconducting transition temperature: Interacting Fermi gas and phonon mechanisms in the nonadiabatic regime. *Phys Rev B* **93**, 054517 (2016).

104. Migdal, A. B. Interaction between Electrons and Lattice Vibrations in a Normal Metal. *Sov. Phys.–JETP* **7**, 996 (1958).